The flow in the mixing region of a jet

By MARC A. KOLPIN
Massachusetts Institute of Technology†

(Received 19 March 1963 and in revised form 6 September 1963)

The object of this work was to investigate experimentally the structure of the early shear layer of high-speed jets and its relation to the mechanism of noise generation. Of special interest was the question of the existence of periodic fluctuations in the velocity field. The experimental investigation is divided in three parts.

(*a*) Optical observation of the jet flow by means of the shadowgraph technique.

(*b*) Measurement of mean Mach number and temperature profiles.

(*c*) Survey by means of hot-wire of the component of the fluctuating velocity field in the mean flow direction.

The shadowgraphs show very interesting features of the breakdown process of free shear layers, but fail to show any propagation of strong acoustic disturbances in the near pressure-field.

Mean profile measurements show that the flow field in the range $1 \leqslant x/d \leqslant 4$ develops in a conical fashion, i.e. the mean profiles in Mach number and temperature can be expressed in terms of a single conical variable $\eta = (2r-d)/2x$. The fluctuating velocity field is described in terms of the intensity of turbulence, its spectral distribution, and two-point space-time correlation functions. Similarity laws are given for the power spectra and the space-time correlation functions. On the cylinder $r = \frac{1}{2}d$, the convection speed of the turbulent field is different for the different eddy sizes, varying from the local mean speed for small eddies to $\frac{1}{2}U_{\text{exit}}$ for the large eddies. Measurements of the angular correlation function are reported which show no correlation of the fluctuations across the jet diameter.

1. Introduction

The measurement of the flow in the mixing region of a high-speed round jet reported here was initiated as part of a general study of the problem of aerodynamic noise. If we define a theory of jet noise as the link between the fluctuating flow field and the sound field far from the source, a description of the former in terms of similarity parameters is mandatory and at this stage of understanding of the problem should always be made available along with the acoustical measurements. Apparent inconsistencies between reported measurements could probably be reconciled if more details about the source of the field were given.

If it is now agreed that the bulk of the noise is produced by the flow region within a few diameters downstream of the nozzle, that is in the region of high

† Present address: Aerospace Corporation, El Segundo, California.

shear rate, the detailed mechanism of sound production is still incompletely understood. Most analyses are based on the assumption that the mean velocity and temperature distribution in the free shear layer and the structure of the turbulent field are well known and amenable to simple analytical representation. Unfortunately we are far from this situation and a great number of questions need to be answered. For example, it would be of particular interest to gain some information about the existence of regular fluctuations in the turbulent field. Such a pattern would be a most efficient sound generator and would provide a model easily accessible to analysis (Mollo-Christensen 1961).

Experimental investigations of jet flows are quite numerous but very few deal with the early part of the free shear layer. Owing to a lack of complete data in terms of Mach number and temperature profiles, comparison with previous measurements are not possible at this time. The first complete investigation was carried out in 1956 by Laurence (1956). He reported mean velocity profiles, intensity, spectrum and correlation of the turbulent field of a 3·5 in. round jet at different exit Mach numbers. From the point of view of sound emission from an air stream, the knowledge of the space-time correlation of the turbulent field is of prime importance. Indeed, the overall intensity of the sound field will be made up of the R.M.S. contribution of each correlated volume and its directionality will be mostly influenced by their convection speed. The obvious step to take was then to extend Laurence's work in this direction and to look for similarity relations so as to scale the problem properly.

While this work was under way at the Massachusetts Institute of Technology, a very similar and independent effort was carried out at the University of Southampton by Davies, Fisher & Barratt (1963). Unfortunately, this paper came to our attention too late for the measurements reported there to be compared in detail with ours. It can be said, however that their work is in general agreement with our results.

The investigation reported in this paper is divided in three parts:

(1) a preliminary investigation of the flow field and pressure field near the jet boundaries carried out by means of shadowgraph pictures;

(2) measurements of mean Mach-number and static temperature profiles made in jets of two different diameters (1 and $\frac{1}{2}$ in.) at exit Mach numbers of 0·8, 0·9, 0·95 and at two stagnation temperature levels;

(3) an investigation of the u-component of the turbulent field by means of hot wires and associated equipment.

The measurements are discussed and we show that they can be expressed in terms of simple combination of parameters.

The description of the flow given here is also meant to support acoustical measurements reported by Mollo-Christensen, Kolpin & Martuccelli (1963).

2. Experimental apparatus

2.1. *Flow-producing apparatus*

The flow-producing system, the main components of which are dry compressed air, a heater, a temperature controlled settling chamber and two interchangeable,

geometrically similar convergent nozzles, is sketched in figure 1. A detailed drawing of the 1 in. nozzle is shown in figure 2. Note the provision to remove the boundary layer at the point where the two nozzles start to be exactly similar.

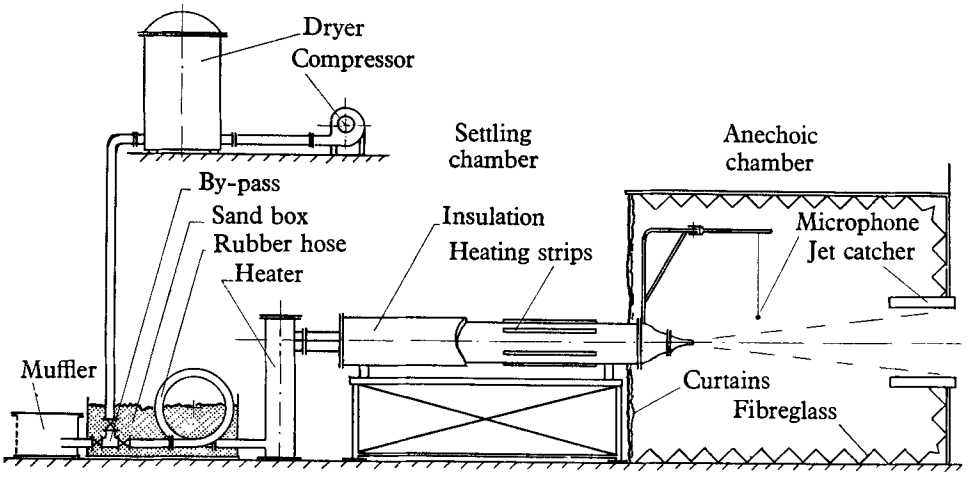

FIGURE 1. Flow apparatus.

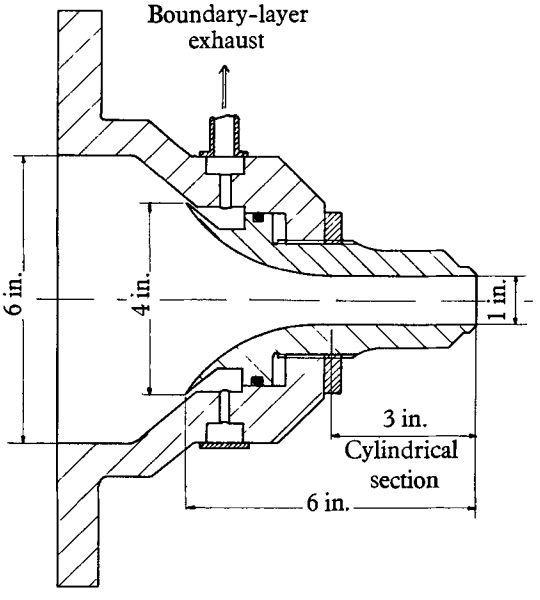

FIGURE 2. Jet nozzle, 1 in. diameter.

However, it was found that, to achieve axial symmetry of the velocity profiles, a perfectly symmetrical suction was necessary. Unfortunately, this was not possible with the actual design used so that all runs were made with the suction lips tightened against the cone.

The boundary layer on the nozzle wall was laminar and very thin, of the order of 3 % of jet diameter. The turbulence level $(\overline{u^2})^{\frac{1}{2}}/U$ in the settling chamber before the contraction leading to the jet was below 10^{-3}.

2.2. *The optical arrangement*

The shadowgraph pictures were taken at night by means of an electronic flash-light placed at right angles to the flow at a distance of 230 cm. The distance between the jet and the photographic plate was varied from 25 to 100 cm. to obtain the best possible resolution. No real difference in the quality of the pictures was found for distances ranging from 65 to 90 cm. The light source was an Edgerton, Germeshausen and Grier 'Point Lite Source' with a flash duration of 10^{-6} sec. The physical size of the arc being too large for a true point source, it was masked by a thin aluminium plate with a 1 mm pin-hole drilled in it. The shadowgraphs were taken directly on the photo films.

2.3. *Method of measurements and recording*

The main building blocks of the measurement and recording system are shown in figure 3. The system was made very flexible and could be modified and expanded to meet our measurement requirements. The traversing mechanism shown in figure 4, plate 1, was of a design that permitted us to move the probes freely and independently along the three cylindrical co-ordinates x, r and θ. The alignment of the traversing mechanism was made by recording total pressure profiles and modifying its position until the axes of symmetry of all the profiles were on a straight line in space.

The total-head probe had a frontal area of $0{\cdot}015 \times 0{\cdot}092\,\mathrm{cm}^2$ and the opening was approximately $0{\cdot}005 \times 0{\cdot}075\,\mathrm{cm}^2$. No corrections were introduced with regard to the influence of the high transverse velocity gradient and turbulence. The temperature profiles were measured with a very small iron-constantan unshielded thermocouple. The junction was made by flash welding the tips of the wires together. The thermocouple reading was calibrated in the potential cone of the jet where the total temperature was accurately known. A plot of recovery temperature *vs.* total temperature could thus be drawn for different Reynolds numbers. The accuracy of the measurement is within $\pm\frac{1}{2}^\circ$C. The pressure and temperature probes could be located to within 0·005 cm. Their position was recorded electrically by a ten-turn potentiometer and fed to the X-axis of an (X, Y)-plotter. The pressure was recorded by an unbounded strain-gauge transducer which was connected to the Y-axis of the plotter. The system had an overall accuracy of 1 % of full scale which was considered satisfactory for our purpose.

The hot-wire probes were made by gluing with a bakelite cement two chrome alloy needles, 0·05 cm in diameter, to a wedged brass support. They extended 0·25 cm in front of the leading edge of the wedge and were spaced approximately 0·1 cm apart. The sensing wire was made of $3{\cdot}81\,\mu$ tungsten wire and was fastened to the prongs of the needles by the copper-plating-soldering technique.

A microscope was used to observe the hot wire while in operation. Vibrations

could thus be detected and eliminated. The microscope was also used to relocate the probe after a wire failure. Repeatability of the position of the wire was within $\pm 0{\cdot}0025$ cm. The constant-current hot-wire sets used in this investigation are commercially available and are manufactured by Shapiro and Edwards, South

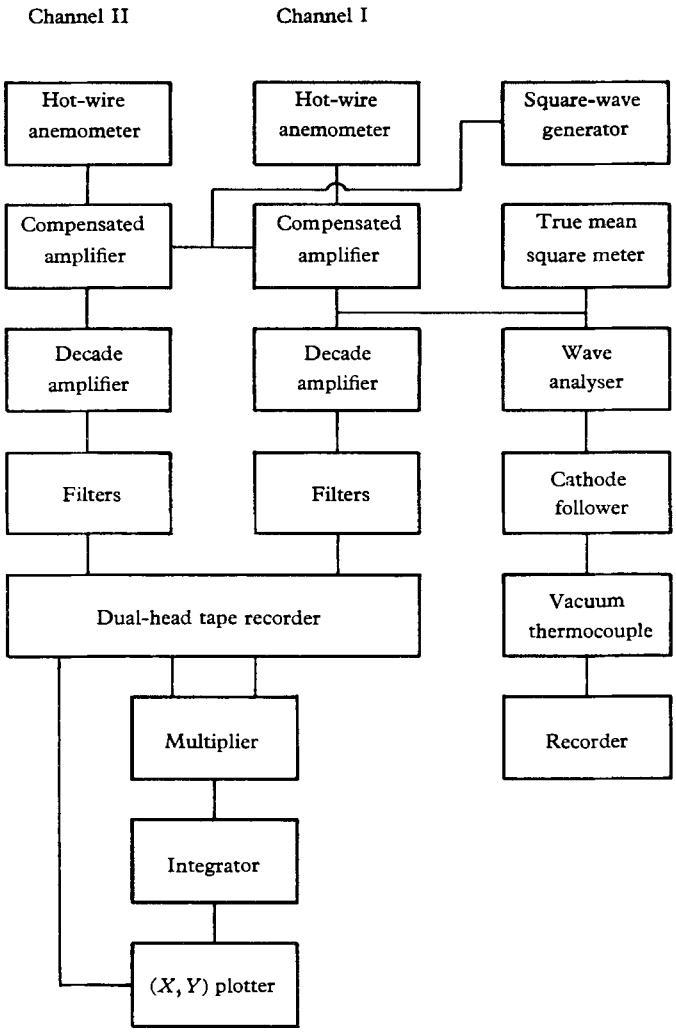

FIGURE 3. Block diagram of the analogue data recording system.

Pasadena, California. The floor-to-ceiling ratio of the amplifier being very high, the input circuit noise had to be chopped above 80 kc/s when the amplifier was compensated.

The automatic recording spectrum-analyser and the correlation computer have been described in detail elsewhere (Kolpin 1962). The power pass band of the spectrum analyser was constant (25 c/s, measured as the width of an equivalent rectangular spectral window) over the full range from 30 c/s to 50 kc/s. The

correlation computer was made of a modified Ampex tape recorder, a Philbrick analog multiplier (Model MU/DV), an integrator made of two chopper stabilized Philbrick plug-in amplifiers (model K2-P and K2-W) and an (X, Y)-plotter. The useful range of the computer extended from 50 c/s to 12 kc/s. Provision was made to allow both hot-wire signals to be filtered by Krohn–Hite variable band-pass filters before they entered the computer.

2.4. *Co-ordinate system and nomenclature*

A cylindrical co-ordinate system is used to describe the measurements. The x co-ordinate is measured along the jet axis, the r co-ordinate being perpendicular to it. The data are plotted in terms of the non-dimensional variable $\xi = x/d$ and $\eta = (r - \frac{1}{2}d)/x$ where d is the jet diameter. The wire separation in the correlation measurements is expressed as $\Delta\xi = \Delta x/d$ and $\Delta\eta = \Delta r/d$. The characteristic time is taken to be proportional to x/U_{exit}. Reduced frequency ν^* and delay time τ^* then becomes $\tau^* = \tau U_{\text{exit}}/x$ and $\nu^* = \nu x/U_{\text{exit}}$. Other notation used in this paper includes: Re, the Reynolds number based on the jet diameter; M, the Mach number; U, the local mean velocity; u, the axial component of the turbulent velocity vector; u', the R.M.S. of u. The subscript 'exit' refers to conditions in the plane $x = 0$.

2.5. *The domain of investigation*

The ideal situation would have been to have investigated the flow for M_{exit} near unity where most of the acoustical measurements were made. Mean flow and optical measurements are performed quite easily in these conditions. Unfortunately, the use of hot wires in the high subsonic régime at atmospheric pressure is no simple matter. The high dynamic loading of the wire compounded with the problem of dust particles that cannot be filtered out in a free jet, and our very limited knowledge of the laws of heat transfer in this régime, made it impossible for us to operate the wire in these conditions. Indeed, for $M_{\text{exit}} > 0{\cdot}5$, the time required to calibrate each individual wire and then make measurements at different values of the overheating parameter so as to separate the different fluctuation modes is much too large compared to the life time of the wire.

For very practical reasons, pertaining to the extreme difficulty of making X hot-wire probes of very small size operating at high dynamic loading, we investigated only the behaviour of the axial component u of the fluctuating velocity vector. It will be shown that a great deal of information can be obtained in this manner and will justify *a postiori* our emphasis on the u-component alone.

The use of constant-current hot-wire sets introduced another limitation. Hinze (1959) has shown that the use of the linear approximation in analysing the response of a hot wire to turbulent fluctuations leads to an error of 10 % in evaluating the measured intensity for a value of $u'/U = 0{\cdot}2$. If we put at 15 % the maximum tolerable error in intensity measurement, all measurements for which $u'/U \geqslant 0{\cdot}25$ have to be disregarded. From these remarks, one can see that the extent of the domain of investigation in space and velocity is totally controlled by the available experimental technique. Its limits are given by

$$\eta \leqslant 0, \quad 1 \leqslant \xi \leqslant 6, \quad M_{\text{exit}} \leqslant 0{\cdot}5.$$

3. Experimental results

3.1. *Optical observations*

The questions we were interested in were the following:

(*a*) Is some kind of regular pattern to be observed in the turbulent flow?

(*b*) Is it possible to detect strong sound waves with a sharp front indicating the possible presence in the shear layer of disturbances moving supersonically with respect to the still air?

(*c*) What is the maximum exit Mach number where the flow remains free of shocks?

Pictures taken at Mach numbers of 0·8, 0·875, 0·95, 0·98 with the 1 in diameter nozzle and at Mach numbers of 0·3, 0·45, 0·60, 0·90 with the $\frac{1}{2}$ in. nozzle are reproduced in figure 5, plates 2 and 3 and figure 6, plates 4 and 5. The very dark silhouette on the left is the nozzle shadow and the flow direction is from left to right.

The pictures can be separated into two categories:

(*a*) *Low Reynolds number*, $Re < 182{,}000$. This flow régime is not very important as far as sound emission is concerned. These pictures were taken mostly because of their usefulness in the study of free-shear-layer transition. They are believed to be unique on the subject. The boundary layer at the exit is laminar, the transition to turbulence taking place between 0·4 and 0·8 cm downstream of the lips. This corresponds to a transition Reynolds number based on this distance of 60,000. Liepmann & Laufer (1947) indicated a Reynolds number of 70,000.

The wave patterns that can be observed are the Tollmien–Schlichting waves leading to turbulence. For low velocities, the waves appear to be essentially two-dimensional but they are not correlated around the jet. Transition seems to take place in a series of partially independent two-dimensional layers. This could explain the good agreement between the two transition Reynolds numbers mentioned above. As the speed is increased, they show more of a three-dimensional character especially just before breaking into random fluctuations. At the same time, the transition line moves towards the nozzle lips, which is to be expected since the boundary layer becomes less stable with increasing Re. These pictures indicate that the last phase of transition is not unique. Some waves break by suddenly rolling on themselves, some by creating very short-scale wave-interference patterns. Transition takes place in such a short distance that the concept of a turbulent spot being convected downstream while spreading sideways seems difficult to apply here.

(*b*) *High Reynolds number*, $Re > 182{,}000$. The boundary layer at the exit is still laminar, the transition to turbulence occurring soon after the shear layer becomes free. The transition line, although well defined, is far from straight. Despite the highly polished nozzle wall, it was impossible to control completely the location of transition, part of it, at higher M_{exit}, taking place in the nozzle itself. This fortunate fact allows us to observe the transition of a laminar and a turbulent free shear layer together. It is very interesting to note the occurrence of finite amplitude waves in the laminar region of the flow. Their wavelength appears to be of the order of 2–3 mm. The waves can be observed for one to one

and a half wavelengths before breaking down. If the boundary layer is turbulent, the transition from boundary layer to free-shear-layer flow is much more gradual and does not seem to involve any instability mechanism as occurs in the laminar case. The fluctuating edges of the jet are clearly seen and fit the model given by Townsend (1956). The double structure of turbulent shear flow is evident and the diffusion of the turbulent field into the still air by the action of the large eddies is approximately proportional to the free-layer thickness: unexplainable up to now is the appearance of horizontal lines in the laminar part of the free shear layer. It was first thought that these lines were caused by some kind of light reflexion on the nozzle walls, but pictures taken without the flow failed to show them. Hence they are believed to indicate variations in density with respect to the circumferential co-ordinate, and would thus reflect the three-dimensional character of the shear layer before transition. These lines and the waves mentioned above point to a region of the flow where a very valuable investigation could be carried on. Although probably not directly related to the mechanism of noise generation, information could be obtained concerning the transition in a free shear layer or the generation of turbulence by turbulence, depending upon the state of the boundary layer.

The picture of the turbulent region failed to show any regular pattern for all Mach numbers. Note the way large eddies are formed very close to the nozzle lips, approximately within 1 diameter. They seem to be formed by a sudden rolling of the flow on itself. This can be observed particularly well on the pictures for $M_{\text{exit}} = 0{\cdot}9$. No sound wave or weak shocks emanating from the jet can be observed in the picture of the still air. It has been shown by Hamitt (1961) that strong oscillations of the jet radiate disturbances which can be detected by the shadowgraph technique; from which we may conclude that, if they exist the oscillations of the shear layer are of rather weak amplitude. Even the initial curling does not radiate an appreciable amount of energy.

The picture taken at $M_{\text{exit}} = 0{\cdot}98$ shows weak shocks appearing at the exit. This gave us the upper limit in Mach number and no tests were conducted at this speed or above.

3.2. *Mean temperature profiles*

The mean temperature profiles were measured at $M_{\text{exit}} = 0{\cdot}8$ and $0{\cdot}9$ and at two temperature levels:

1. 'The cold jet', with the air in the settling chamber at room temperature.
2. 'The hot jet', with the air at 90 ° above room temperature.

The jet was 1 in. in diameter and the thermal boundary layer on the nozzle wall was of the same order of magnitude as the viscous boundary layer. The average T_{atm} was 300 °K. Figure 7 shows the mean static temperature distribution in the mixing zone for $M_{\text{exit}} = 0{\cdot}9$.

It is apparent that for the early shear layer which extends up to $\xi = 4$, the similarity with respect to η is achieved within experimental error. Variation of M_{exit} does not produce measurable difference in the profiles so that in the range we have investigated M_{exit} is not a significant variable.

3.3. *Mach-number profiles*

Profiles of mean Mach number were taken at three different exit Mach numbers ($M_{\text{exit}} = 0{\cdot}8,\ 0{\cdot}9,\ 0{\cdot}95$) and two temperature levels. The measuring stations were at $\xi = 0, 1, 2, \ldots 6$. The $\frac{1}{2}$ in. and 1 in. nozzles were used. The dimensionless boundary-layer thickness $\delta^* = \delta/d$ at the exit was of the order of 30×10^{-3}.

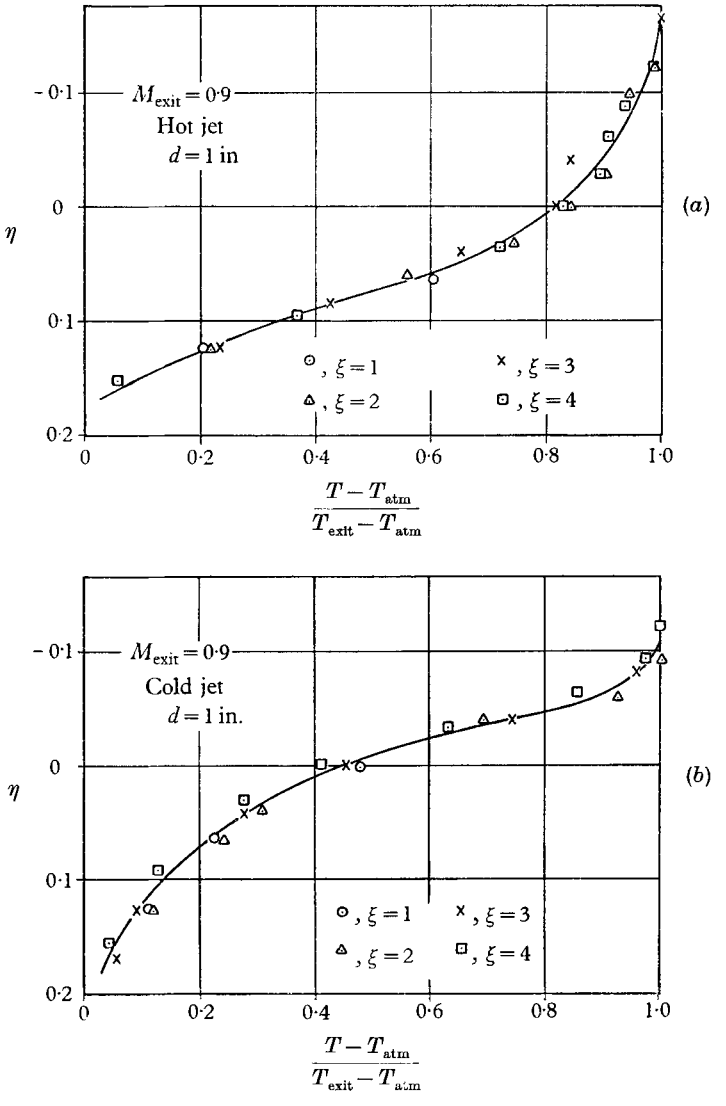

FIGURE 7. Mean static temperature profiles showing similarity for hot and cold jets.

Figure 8 shows some typical mean Mach-number distributions across the mixing zone. The similarity in η, for each nozzle diameter taken separately, is very good. In figure 9, one similarity profile is shown to hold for different M_{exit} at constant ξ and d. However, the similarity in the profile breaks down when

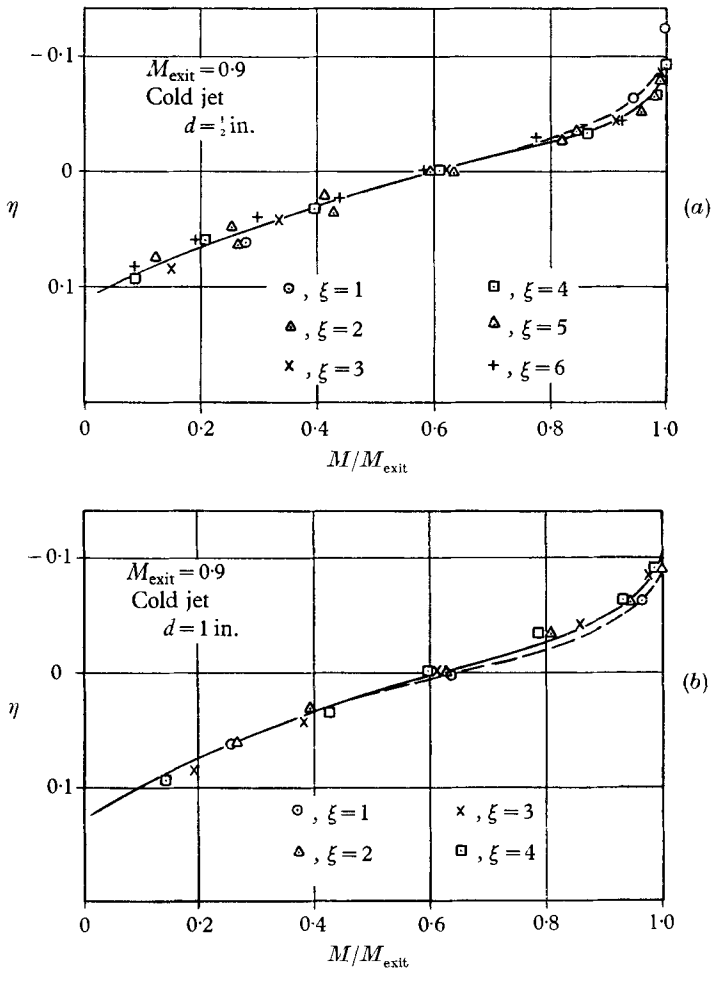

FIGURE 8. Similarity of Mach-number distribution across the jet.

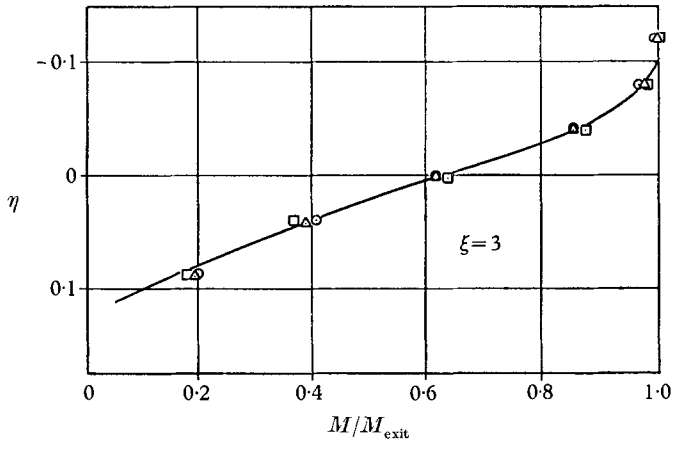

FIGURE 9. Comparison of M/M_{exit} profiles for different M_{exit} and axial locations: $d = 1$ in. ⊙, $M_{exit} = 0{\cdot}8$; △, $M_{exit} = 0{\cdot}9$; □, $M_{exit} = 0{\cdot}95$.

one goes from the 1 in. to the $\frac{1}{2}$ in. nozzle. Figure 10 indicates that if the spreading rate of turbulence in quiet outside air is the same for both nozzles, the spreading rate toward the centre-line of the jet is different. This is reflected by the differing length of the potential cone as shown in figure 11 where the variation of the Mach

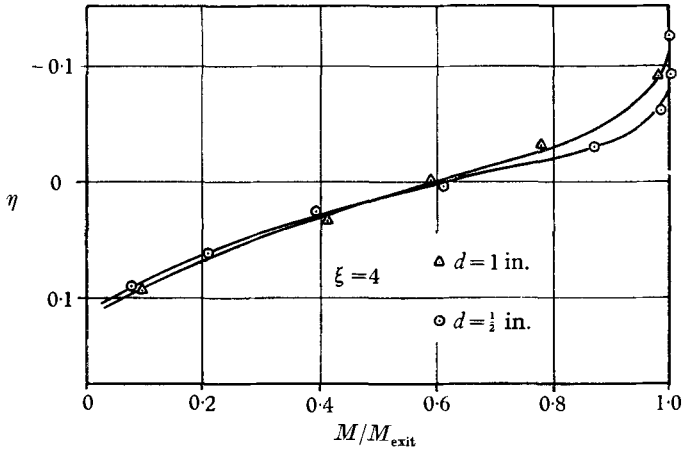

FIGURE 10. M/M_{exit} *vs* η at constant ξ for different *Re*.

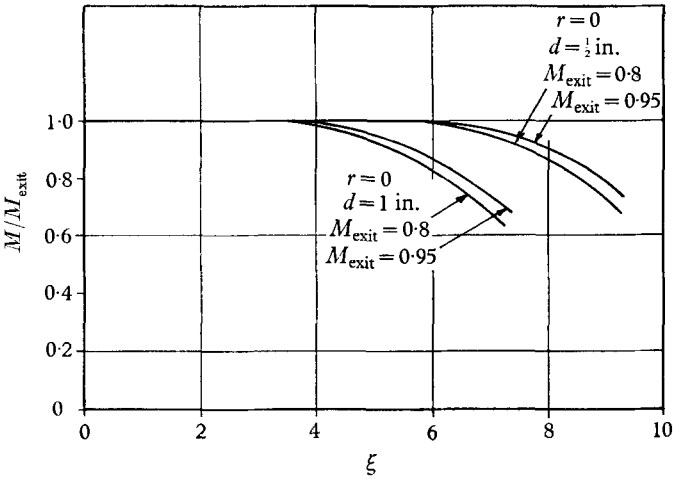

FIGURE 11. M/M_{exit} *vs* ξ on the jet axis.

number on the jet axis is plotted *vs* ξ. The ratio $M(r = 0)/M_{exit}$ is equal to unity in the cone and decreases in the turbulent region. From the point of view of jet noise, this means that the region of high shear is relatively larger for jets of small diameter and that noise output of such jets cannot be extrapolated to larger diameter without questions.

3.4. *The intensity of turbulence*

The intensity of turbulence was measured along the line $\eta = 0$ for different ξ positions and also for $\xi = 2$ and $\eta \leqslant 0$. The intensity, given as a percentage of

the exit velocity is shown in figures 12 and 13. Within experimental accuracy, we can say that the intensity distribution is a function only of η and U_{exit} and that, above a certain Re, the jet diameter plays no role in the description of the turbulent field. Comparison with Laurence's experiment is good in view of the great difficulty of compensating the amplifier properly for the thermal lag of a hot-wire operating in a flow of very high turbulent intensity.

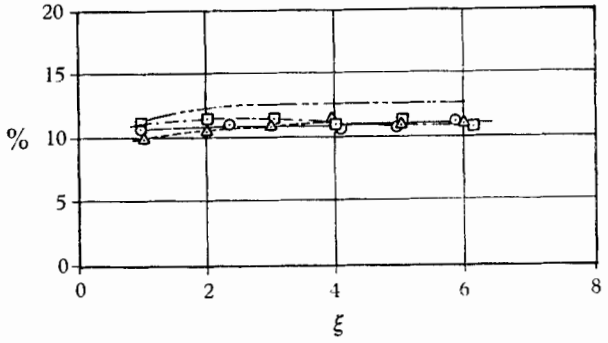

FIGURE 12. Intensity of turbulence as percentage of core velocity. $M_{\text{exit}} = 0{\cdot}3$, $\eta = 0$; $M_{\text{exit}} = 0{\cdot}5$, $\eta = 0$; ⊙, $d = 1$ in.; △, $d = 1$ in.; ⊡, $d = 0{\cdot}5$; —·—··, $d = 3{\cdot}5$ (Laurence).

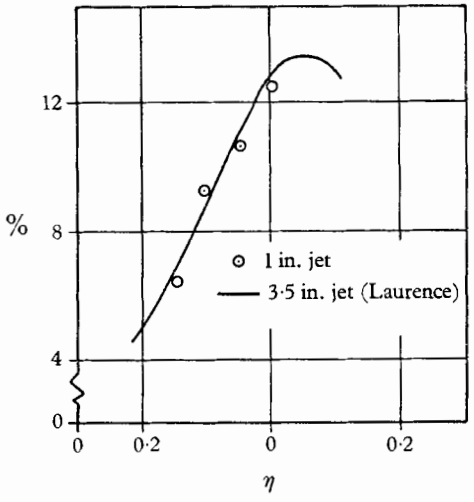

FIGURE 13. Lateral profile of the intensity of turbulence as percentage of core velocity. $M_{\text{exit}} = 0{\cdot}3$, $\xi = 2$.

3.5. *The spectrum of turbulence*

A spectral analysis of the hot-wire signal was performed while doing the intensity measurements. The intensity being independent of ξ, the spectral function was normalized to give

$$\int_0^\infty \Phi(\nu)\, d\nu = 1. \tag{1}$$

In figure 14 all the spectra are reduced to a single curve by plotting them in the form

$$\Phi U_{\text{exit}}/x = \phi(\nu^*). \tag{2}$$

Note the good agreement with Laurence's data.

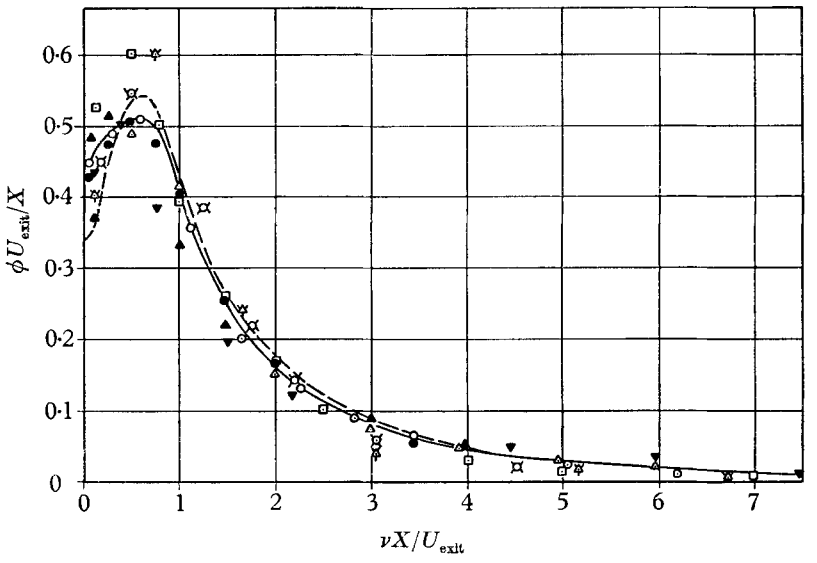

FIGURE 14. Similarity in the power spectra for $\eta = 0$. – – –, Laurence: $M_{\text{exit}} = 0{\cdot}3$, $\xi = 2{\cdot}29$, $\eta = 0$, $d = 3{\cdot}5$ in.

ξ	$M_{\text{exit}} = 0{\cdot}3$ $d = 1$ in.	$M_{\text{exit}} = 0{\cdot}3$ $d = \frac{1}{2}$ in.	$M_{\text{exit}} = 0{\cdot}5$ $d = 1$ in.
1	⊡	—	⊠
2	⊙	⊙	✳
4	△	△	
6	—	▼	—

Here, as for the mean profiles we see that the only relevant variables are the exit velocity and the axial distance x. Turbulence is generated by the shear flow at the lower end of the spectrum and convected downstream where the high frequencies are losing their energy by dissipation. An illustration of the process is given on figure 15 where Φ is plotted *vs* ξ with ν as a parameter. $\Phi(\nu)$ being a measure of the energy contained in the signal for a small band of frequencies in the vicinity of ν, one can interpret the graph as follows. The fine structure of turbulence is generated in the transitional region $\xi < 1$. If no energy was fed from the mean flow to turbulence and neglecting dissipation, $\Phi(\nu)$ would be proportional to $1/\xi$ so as to conserve the energy flux stored in the turbulent fluctuations. At $\xi = 1$, energy is fed into the fluctuating field only for $\nu \lesssim 5$ kc/s, the higher frequencies simply being convected downstream. As one proceeds downstream, the range of frequencies with increasing energy narrows and more

and more of the turbulence is just drifting and decaying without being fed any energy directly from the shear flow. It is very interesting to note that energy is only fed to wavelengths $\lambda = v/U_{\text{conv}}$ large compared to the shear-layer thickness.

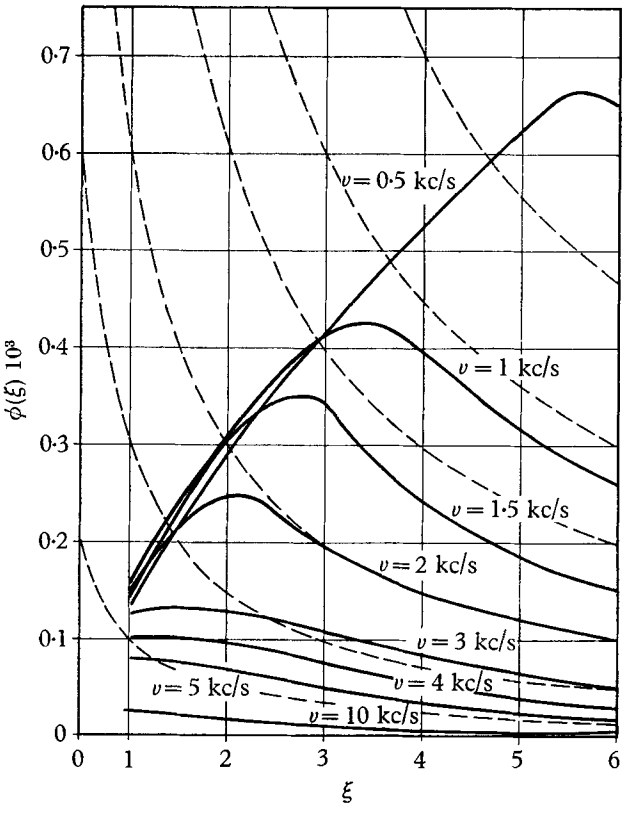

FIGURE 15. Power spectra cross-plotted for running axial co-ordinate and fixed circular frequencies. $M_{\text{exit}} = 0{\cdot}3$, $d = 1$ in., $\eta = 0$.

3.6. *Correlation measurements*

The two-point longitudinal correlation or convariance of the u-component of the velocity fluctuation is defined as

$$R(x, \Delta x, \tau) = \frac{\langle u(x,t)\, u(x+\Delta x, t+\tau)\rangle}{u'(x,t)\, u'(x+\Delta x, t+\tau)}, \tag{3}$$

and the temporal Fourier transform of the autocorrelation as

$$R_{\bar{E}}(x,\tau) = \int_0^\infty \Phi(\nu, x) \cos 2\pi\nu\tau\, d\nu. \tag{4}$$

From the power spectra measurements we have

$$\Phi(\nu, x) = x\phi(\nu^*)/U_{\text{exit}}, \tag{5}$$

or for the autocorrelation

$$R_{\bar{E}}(x,\tau^*) = \int_0^\infty \phi(\nu^*) \cos 2\pi\nu^*\tau\, d\nu^*; \tag{6}$$

we then expect the correlation function to be of the form

$$R = R(x, \Delta x, \tau^*). \tag{7}$$

The structure of the turbulent field being independent of the jet diameter, writing the argument of R in non-dimensional form leads to the functional relation

$$R = R(\Delta x/x, \tau^*). \tag{8}$$

Our measurements of the correlation function show that this form is indeed correct to a first approximation.

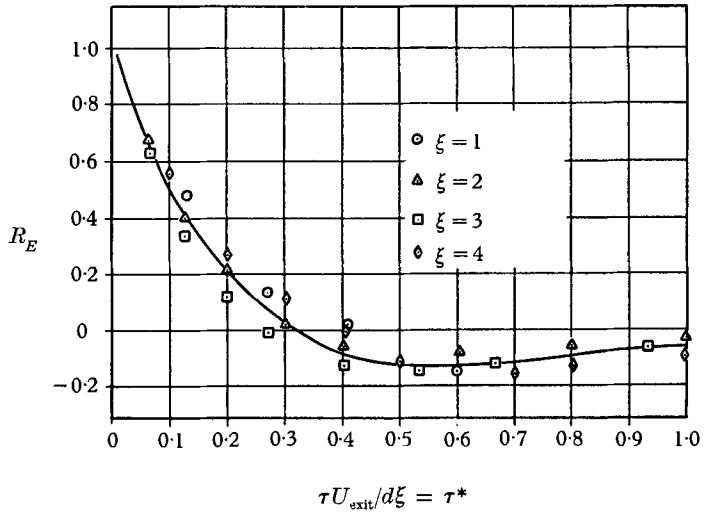

FIGURE 16. Autocorrelation function. $M_{exit} = 0{\cdot}3$, $d = 1$ in., $\eta = 0$.

Experimental results. In figure 16 the function R_E is plotted *vs.* the time delay made dimensionless with the shear rate. The similarity is quite apparent. The negative portion of the curve is probably overestimated because of the inadequate low-frequency cut-off of the correlation computer.

In figure 17 the longitudinal correlation function $R_\xi = R(\Delta\xi/\xi, 0)$ is plotted. The similarity is satisfactory.

Figure 18 shows a comparison of R_E and R_ξ if $\Delta\xi = \tau U/d$. The agreement is surprisingly good in the light of the fact that Taylor's hypothesis should certainly not be valid in this case, the turbulent field not being homogeneous. This reflects only the fact, which we have already discussed in relation to the spectra, that for most wavelengths the evolution of turbulence in the axial direction is slow with respect to the correlation length. The same observation was made by Laurence. A typical measurement of $R(\xi, \Delta\xi, \tau)$ is shown on figure 19. Many measurements were taken in order to check the similarity and we were able to convince ourselves that indeed the functional form $R(\Delta\xi/\xi, \tau^*)$ is reasonably confirmed by experiment. Some examples of similarity are shown on figure 20. Hence, we can use figure 19 tentatively to interpret the meaning of the space-time correlation function. For small wire separations, the turbulent field is

convected at the speed of the local mean velocity. The correlation function is essentially even, the shorter life time of the small eddies rounding off very rapidly the peak of maximum correlation. As the wire separation gets larger, only disturbances of the order of magnitude of the shear-layer width or larger remain correlated. The correlation function slowly changes to the odd shape that it is

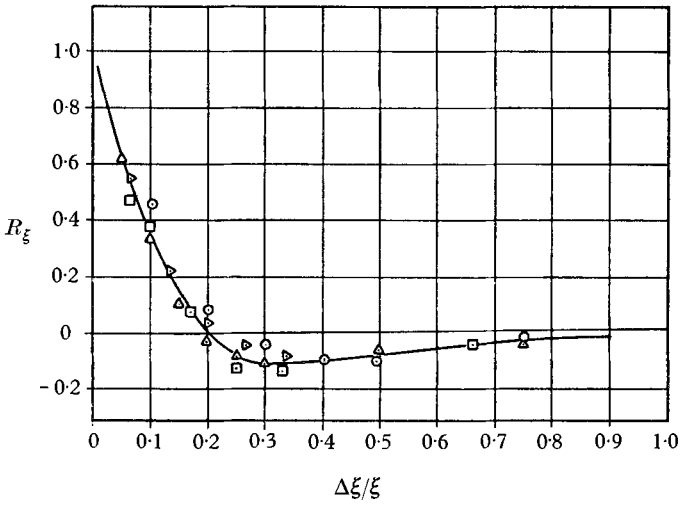

FIGURE 17. Longitudinal correlation function. ⊙, $\xi = 1$, $d = 1$ in.; △, $\xi = 2$, $d = 1$ in.; □, $\xi = 3$, $d = 1$ in.; ▷, $\xi = 3$, $d = \frac{1}{2}$ in.

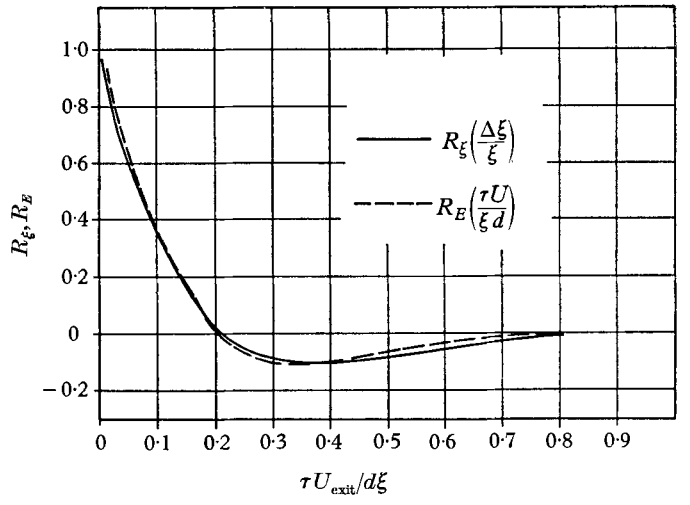

FIGURE 18. Comparison of R_ξ and R_E for $\Delta\xi = \tau U/d$.

going to keep until all correlation disappears. The correlation speed is now smaller and corresponds to $\frac{1}{2}U_{\text{exit}}$. This change in shape of the correlation function indicates a radical difference in the structure of the small and large eddies. The inference of eddy structure from correlation measurement is a rather hazardous task but a close examination of the shadowgraph picture of the flow and our

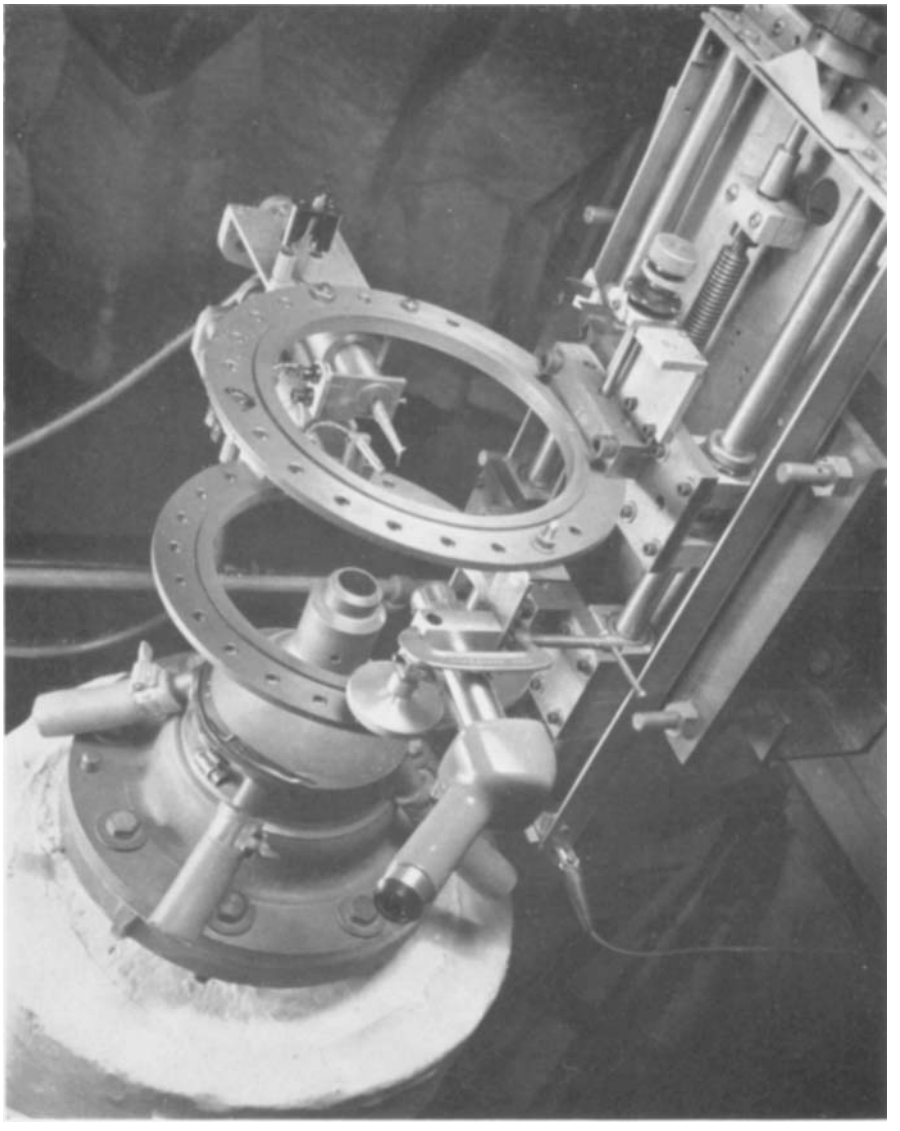

FIGURE 4. Traversing mechanism.

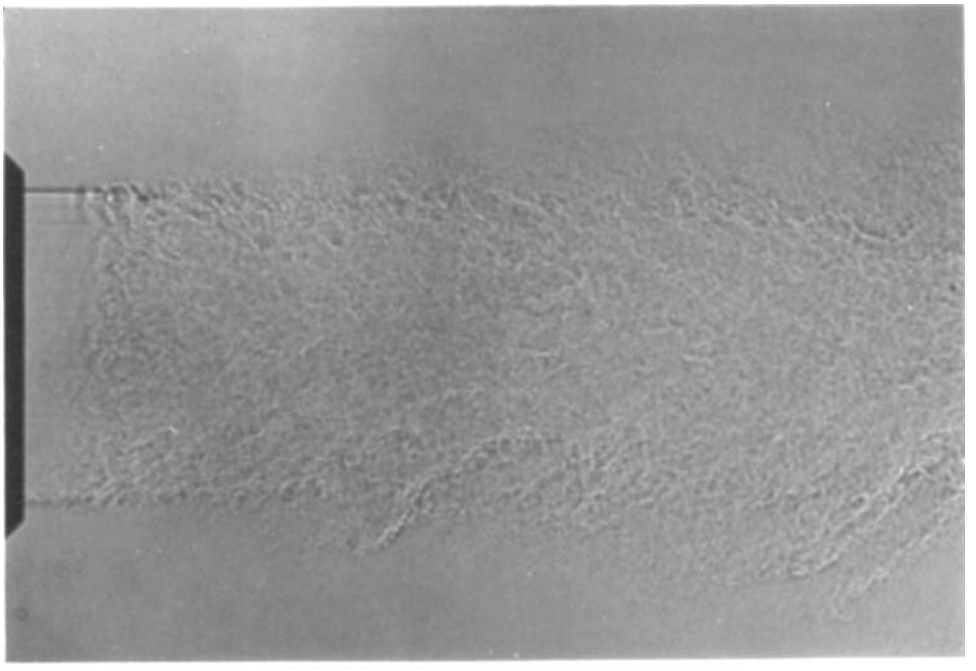

(*a*)

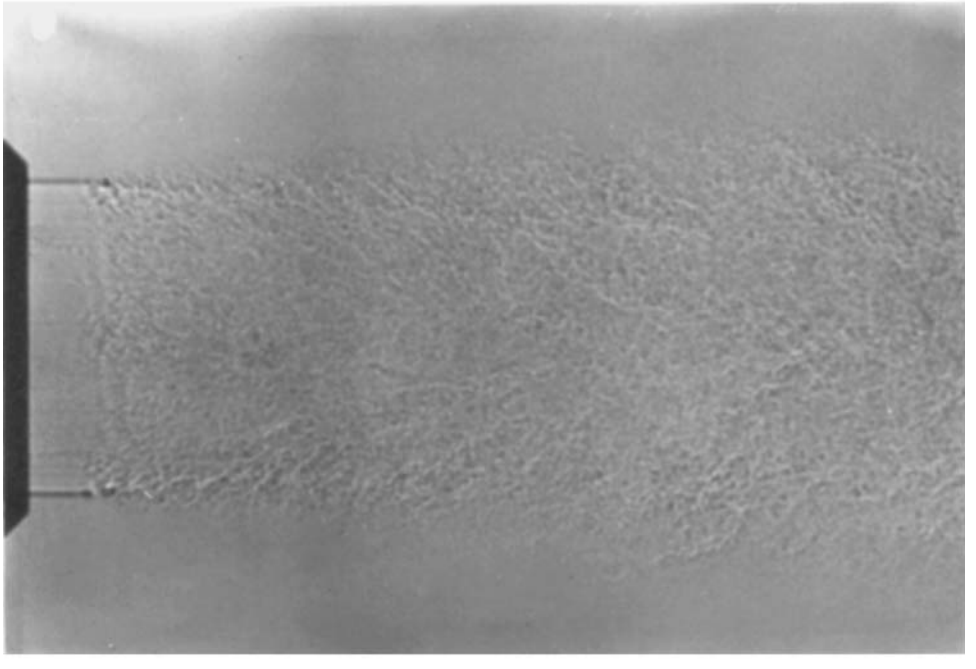

(*b*)

For legend see plate 3.

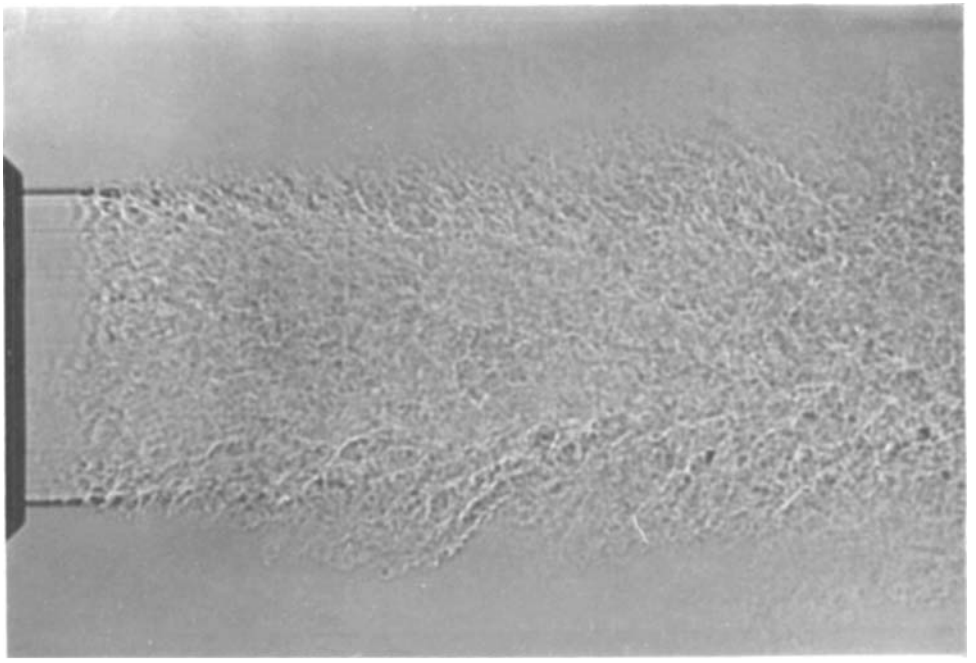

(*c*)

(*d*)

FIGURE 5 (plates 2, 3). Shadowgraphs of the 1 in. jet. (*a*) $M_{exit} = 0{\cdot}80$, $Re = 52{\cdot}4 \times 10^5$; (*b*) $M_{exit} = 0{\cdot}875$, $Re = 5{\cdot}9 \times 10^5$; (*c*) $M_{exit} = 0{\cdot}95$, $Re = 6{\cdot}6 \times 10^5$; (*d*) $M_{exit} = 0{\cdot}98$, $Re = 6{\cdot}85 \times 10^5$.

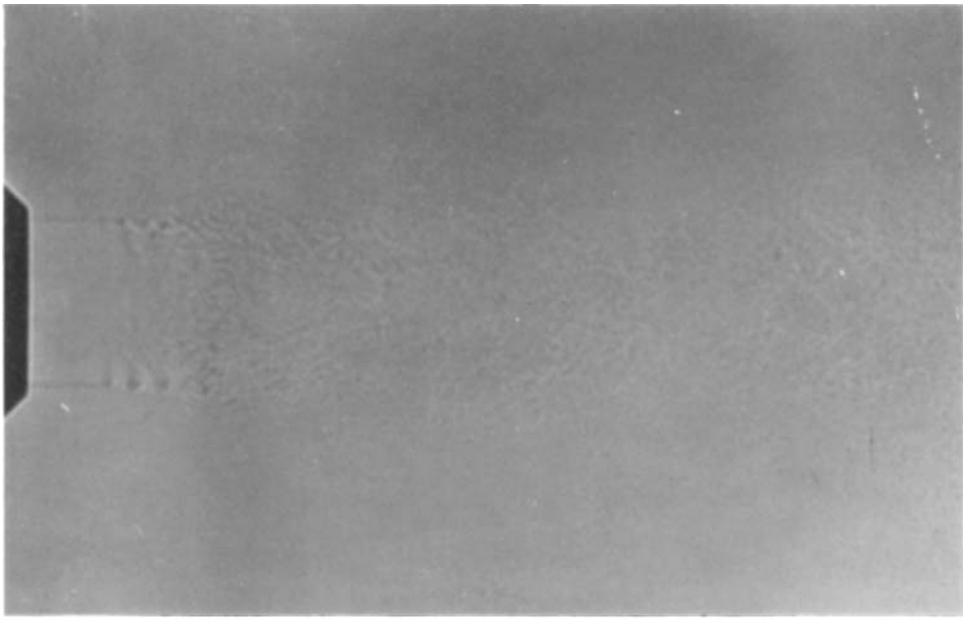

(*a*)

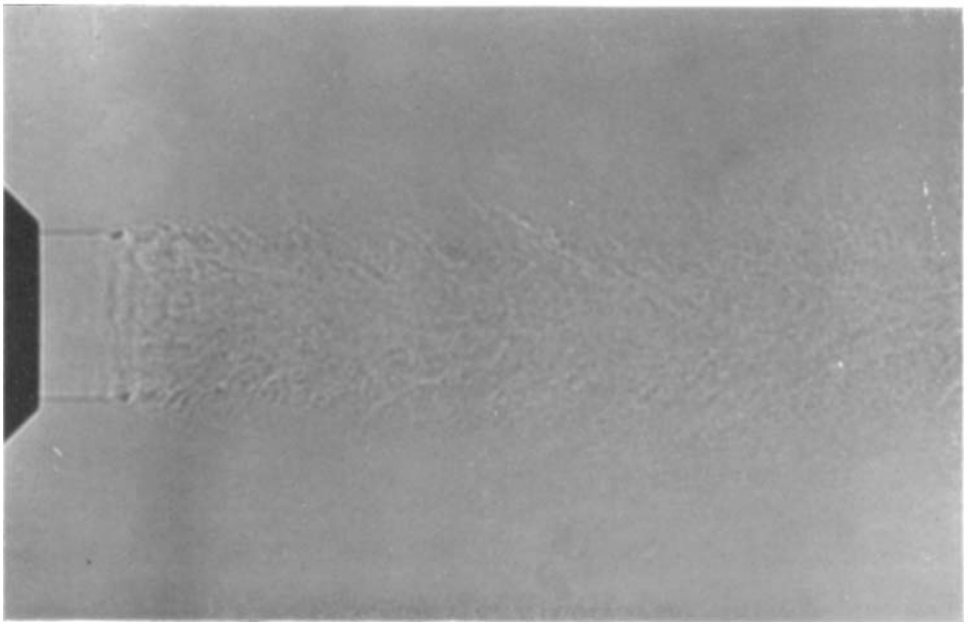

(*b*)

For legend see plate 5.

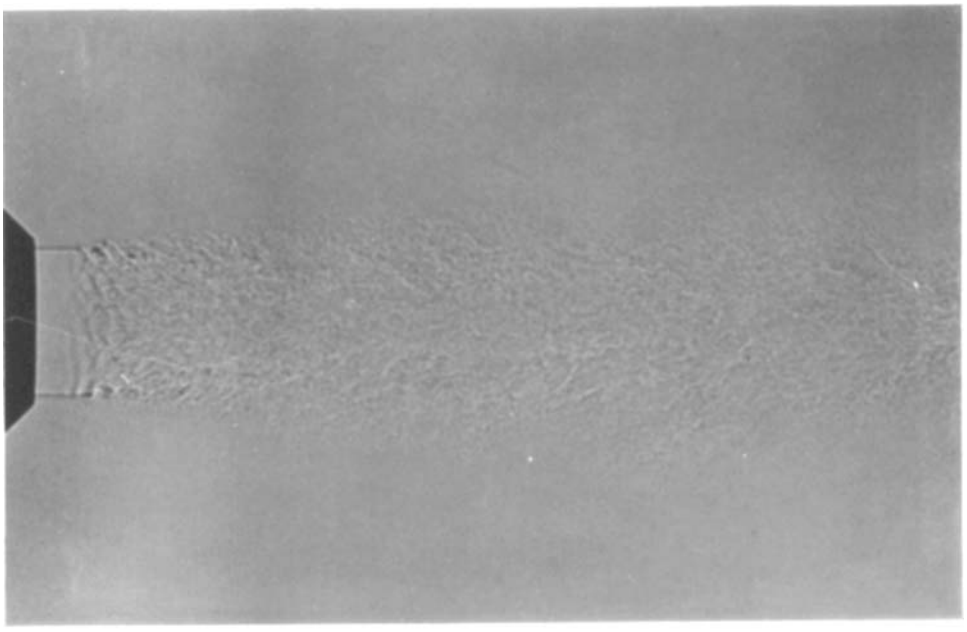

(*c*)

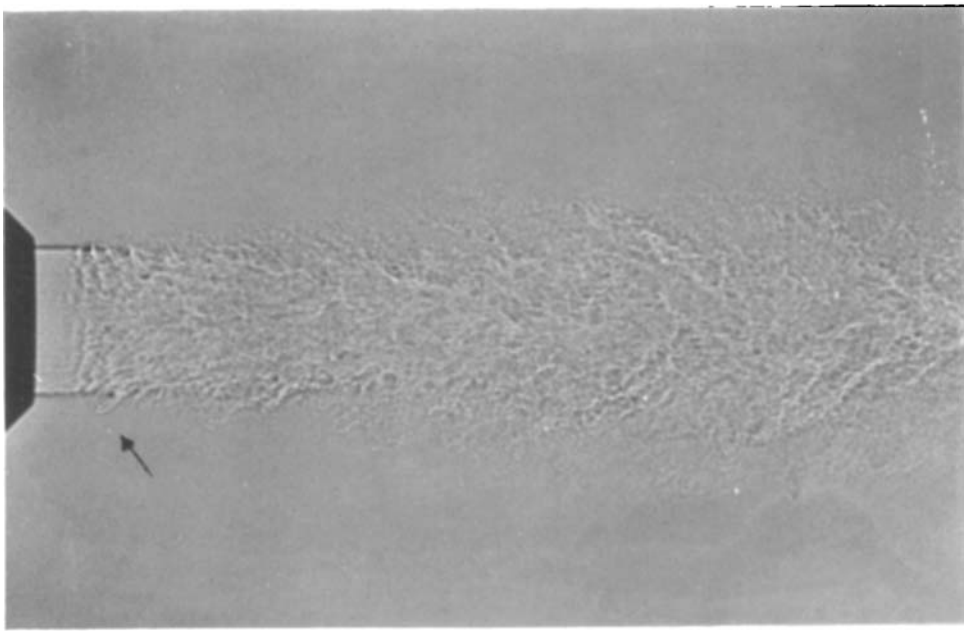

(*d*)

FIGURE 6 (plates 4, 5). Shadowgraphs of the $\frac{1}{2}$ in. jet. (*a*) $M_{exit} = 0{\cdot}30$, $Re = 0{\cdot}85 \times 10^5$; (*b*) $M_{exit} = 0{\cdot}45$, $Re = 1{\cdot}31 \times 10^5$; (*c*) $M_{exit} = 0{\cdot}60$, $Re = 1{\cdot}82 \times 10^5$; (*d*) $M_{exit} = 0{\cdot}90$, $Re = 3{\cdot}3 \times 10^5$.

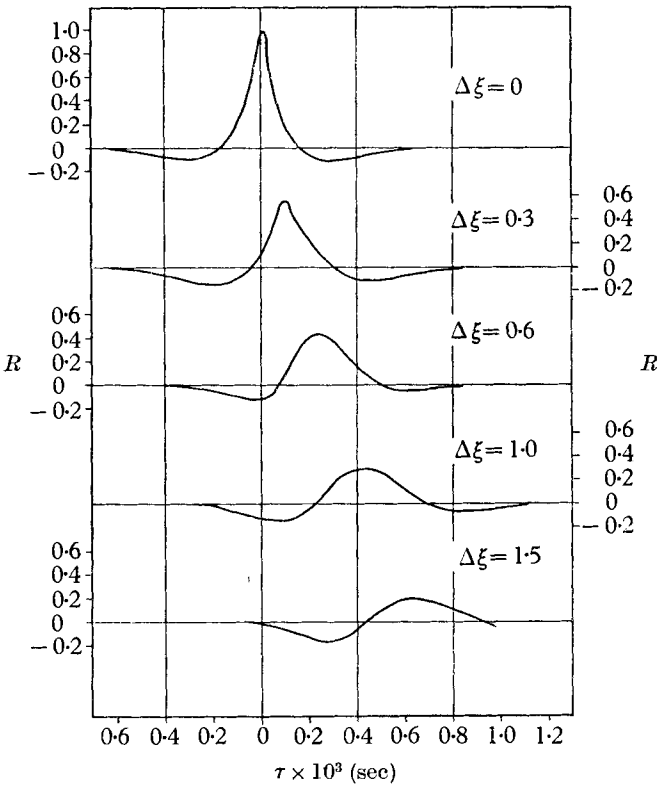

FIGURE 19. Space-time correlation function. $\xi = 2$, $M_{\text{exit}} = 0{\cdot}3$, $\eta = 0$, $d = 1$.

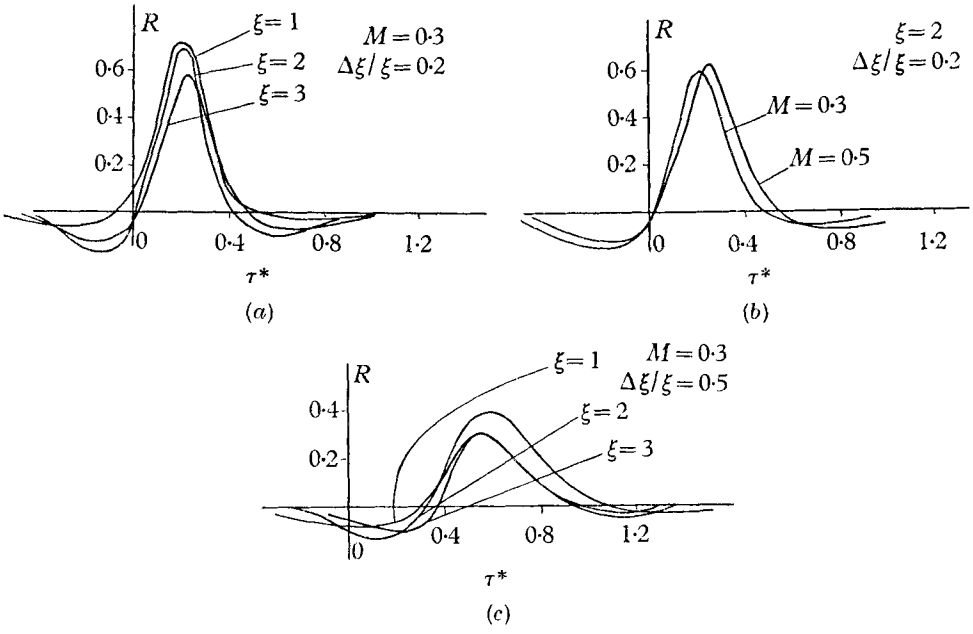

FIGURE 20. Similarity of the space-time correlation function.

limited measurement led us to believe that the large eddies are produced near the nozzle lips by a sudden rolling of the flow on itself and are shed downstream at random times. The creation of a large eddy is a local phenomena as shown by the angular correlation function (figure 22(*b*)). It is too early to decide if Grant's (1958) model for the structure of the large eddies he observed in wakes and boundary layers is also valid here, before more correlation measurements are performed.

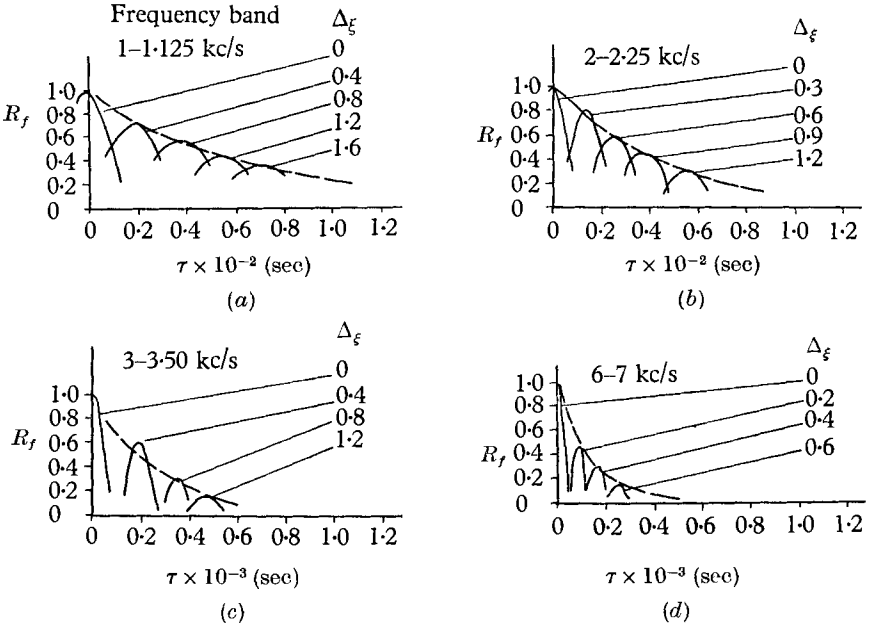

FIGURE 21. Space-time correlations for various frequency bands. $\xi = 2$, $M_{\text{exit}} = 0{\cdot}3$, $d = 1$ in., $r = 0$.

On figure 21 are reproduced space-time correlation functions for various frequency bands. The envelope of the curves is the rate of decay of the eddies as seen by an observer moving with them. The convection speed of the different eddies can also be read off the graph. For all eddies we note a trend for the correlation speed to increase with wire separation. For small separation, the large eddies are convected at half the exit velocity while the small eddies are convected at the local velocity which is slightly higher than $\frac{1}{2}U_{\text{exit}}$.

3.7. *Lateral and angular correlations*

We define the lateral correlation function for zero time delay as

$$R_\eta(\xi, \eta, \Delta\eta) = \frac{\overline{u(\xi, \eta)\, u(\xi, \eta + \Delta\eta)}}{\overline{u'(\xi, \eta)\, u'(\xi, \eta + \Delta\eta)}}, \tag{9}$$

and the angular correlation functions as

$$R_\theta(\xi, \theta, \Delta\theta) = \frac{\overline{u(\xi, \theta)\, u(\xi, \theta + \Delta\theta)}}{\overline{u'(\xi, \theta)\, u'(\xi, \theta + \Delta\theta)}}. \tag{10}$$

All correlation functions were measured at $\eta = 0$.

Figure 22 (*a*) shows that the lateral correlation function is self preserving and can be expressed in the form

$$R_\eta = R_\eta(\Delta\eta/\xi). \tag{11}$$

The measurements of the angular correlation function were performed primarily to investigate possible feed-back of the turbulent field on itself across the laminar core of the jet. Wehrmann & Wille (1958) having shown that transition in a

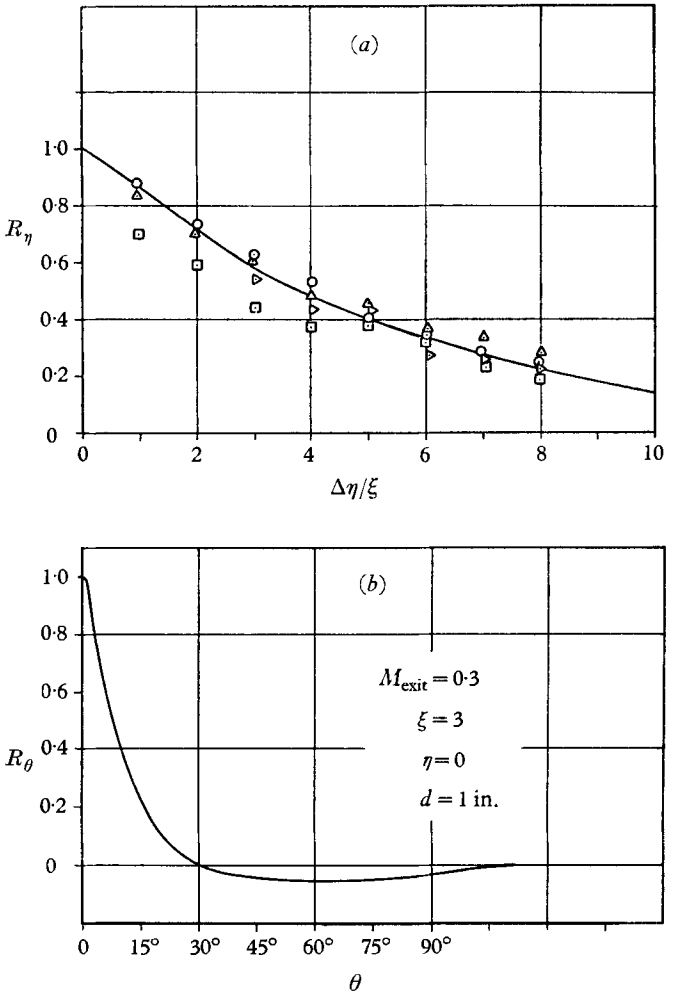

FIGURE 22. Lateral correlation function. (*a*) Wire separation in radial direction. $M_{exit} = 0{\cdot}3$, $\eta = 0$. ⊙, $\xi = 1$, $d = 1$ in.; △, $\xi = 2$, $d = 1$ in.; ⊡, $\xi = 3$, $d = 1$ in.; ▷, $\xi = 3$, $d = \frac{1}{2}$ in. (*b*) Wire separation in angular direction.

laminar annular shear layer was correlated all around it, it was also of interest to see if the eddies would show especially long correlation in the angular direction. Space-time correlation curves were recorded for the wires located at different angular positions for $\xi = 3$ and $\eta = 0$. No correlation of the velocity fluctuation could be detected across the jet diameter. Figure 22 (*b*) shows the angular correla-

tion function for zero time delay. The eddy size is of the order of the shear-layer thickness and there is no indication of an annular structure for the turbulent field.

4. Conclusion

We have shown that the flow field in the mixing region of a jet can be described in terms of a few dimensionless variables. The turbulent field was found to be devoid of any regular velocity fluctuations in time or space. The generation of turbulence, governed by the interaction of the large eddies and the mean flow, is a local phenomenon. Indeed, no long-range correlation was found to exist around the annular shear layer.

The volume over which the space-time correlation of the velocity fluctuation is different from zero can be evaluated. It extends in the flow direction for an approximate length of $1{\cdot}6\xi$ upstream and downstream of the fixed point. Its lateral and angular dimensions are of the order of the shear-layer thickness. The sound fields emitted by each correlation volume being uncorrelated, they can be studied separately and then superposed linearly.

The author wishes to express his gratitude and appreciation to Professor Mollo-Christensen who interested him in this problem and whose enthusiasm and support were important factors in the completion of this work. The investigation was supported by a grant from the National Aeronautics and Space Administration.

REFERENCES

DAVIES, P. O. A. L., FISHER, J. J. & BARRATT, M. J. 1963 Turbulence in the mixing region of a round jet. *J. Fluid Mech.* **15**, 337.

GRANT, H. L. 1958 The large eddies of turbulent motion. *J. Fluid Mech.* **4**, 149.

HAMITT, A. G. 1961 The oscillation and noise of an overpressure sonic jet. *J. Aerospace Sci.* **28**, 673.

HINZE, J. O. 1959 *Turbulence.* New York: McGraw-Hill.

KOLPIN, M. 1962 The flow in the mixing region of a jet. *ASRL TR* 92–3, *Mass. Inst. Tech.*

LAURENCE, J. C. 1956 Intensity, scale and spectra of turbulence in mixing region of free subsonic jet. *NACA TR* 1292.

LIEPMANN, H. W. & LAUFER, J. 1947 Investigation of free turbulent mixing. *NACA TN* 1257.

MOLLO-CHRISTENSEN, ERIK 1961 Some aspects of free shear layer instability and sound emission. *Fluid Dynamics Res. Lab. Memo.* 60–1, *Mass. Inst. Tech.*

MOLLO-CHRISTENSEN, E., KOLPIN, M. & MARTUCCELLI, J. R. 1963 Experiments on jet flows and jet noise, far field spectra and directivity patterns. *ASRL TR* 1007, *Mass. Inst. Tech.*

TOWNSEND, A. A. 1956 *The Structure of Turbulent Shear Flow.* Cambridge University Press.

WEHRMANN, O. & WILLE, R. 1958 Beitrag zur Phänomenologie des laminar-turbulenten Ubergangs im Freistrahl bei kleinen Reynoldszahlen. *Boundary Layer Research.* Berlin: Springer Verlag.